Sensors and Materials, Vol. 35, No. 10 (2023) 4731–4750
MYU Tokyo

S & M 3426

Clinical Performance of Reverse Transcription Loop-mediated Isothermal Amplification COVID-19 Assay on Gold-nanoparticle-modified Screen-printed Carbon Electrode Using Differential Pulse Voltammetry

Munirah Zulhairee,[1,2] Rozainanee Mohd Zain,[2] Adibah Che Mohamad Nor,[2,3] Nur Fadhilah Jafar,[1] Mohd Fairulnizal Md Noh,[2] Mohd Shihabuddin Ahmad Noorden,[3] Anis Nurashikin Nordin,[4] Rosminazuin Ab Rahim,[4] Teddy Surya Gunawan,[4] Lim Ying Chin,[1] Yusairie Mohd,[1] Nur Asyiqin Azman,[1] and Zainiharyati Mohd Zain[1*]

[1]Electrochemical Material and Sensors (EMaS), Faculty of Applied Sciences, Universiti Teknologi MARA (UiTM), 40450 Shah Alam, Selangor, Malaysia
[2]Institute for Medical Research (IMR), National Institute of Health (NIH), Jalan Setia Murni U13/52, Seksyen U13 Setia Alam, 40170 Shah Alam, Selangor, Malaysia
[3]Faculty of Pharmacy, Universiti Teknologi MARA (UiTM), Puncak Alam, Bandar Puncak Alam, 42300 Puncak Alam, Selangor, Malaysia
[4]International Islamic University Malaysia, Jalan Gombak, 53100 Kuala Lumpur, Wilayah Persekutuan Kuala Lumpur, Malaysia

(Received April 17, 2023; accepted July 24, 2023)

Keywords: COVID-19, RT-PCR, RT-LAMP, AuNP/SPCE, differential pulse voltammetry, electrochemical sensor

The World Health Organization (WHO) has recommended real-time reverse transcription polymerase chain reaction (RT-PCR) as the gold standard for coronavirus disease detection. In this study, we aim to validate the clinical performance of reverse transcription loop-mediated isothermal amplification (RT-LAMP) assay on a gold-nanoparticle-modified screen-printed carbon electrode (AuNP/SPCE) using differential pulse voltammetry (DPV) and to compare it with real-time RT-PCR. The electrodeposited AuNP on SPCE was quasi-spherical with a size of ±500 nm. The developed RT-LAMP primer was designed from the GenBank database using the NCBI Multiple Alignment tools and Jalview software. Nasopharyngeal clinical samples were obtained from suspected COVID-19 patients (n = 148). The RT-LAMP products were dropped on the modified AuNP/SPCE under DPV setting, which resulted in current change (ΔI) responses. The positive and negative samples produced significantly different ΔI signals with a p-value <0.0001 at a 95% confidence interval using Student's t-test. The RT-LAMP assay using Au/SPCE exhibited a 30 s response time per analysis. The clinical sensitivity and specificity obtained were 79.7 and 85.1%, respectively, with a detection limit of 0.4 copies μl^{-1}. Hence, this proposed method is suitable for COVID-19 RNA detection in resource-limited settings.

*Corresponding author: e-mail: zainihar@uitm.edu.my
https://doi.org/10.18494/SAM4430

ISSN 0914-4935
https://myukk.org/

1. Introduction

In late December 2019, the world was shocked by the emergence of a novel coronavirus (CoV) that causes coronavirus disease (known as COVID-19). In an effort to curb the spread of the virus, the U.S Food Drug and Administration (FDA) issued the Emergency Use Authorization (EUA) to authorize unapproved drugs and medical devices, including the implementation of real-time RT-PCR, which is a diagnostic laboratory tool recommended by WHO and considered the gold standard for COVID-19 detection.[1,2] It requires a series of procedures involving the amplification of nucleic acids, including reverse transcription, denaturation, primer annealing, and extension.[3,4] However, real-time RT-PCR can only be carried out in certified laboratories with expensive equipment maintenance and trained personnel, and with a turnaround time (TAT) of more than 24 h.[3] In our context, TAT is the time taken from sample extraction up to a result declaration. In addition, the drawback of real-time RT-PCR is that it might lead to high false-negative and false-positive results.[4,5] The term of analysis time here is defined as the operational time taken by an instrument to obtain the output signal. In this study, differential pulse voltammetry (DPV) was used for the detection of SARS-CoV-2's RNA.

DPV can be used to detect viral DNA as it is sensitive to low capacitive current and thus excellent for trace detection.[6] This was proven by Moço *et al.* for the detection of a Zika virus antigen on graphite electrodes modified with the reduced graphene oxide and polytyramine-conducting polymer immobilized with a Zika virus oligonucleotide probe.[7] Furthermore, the electrochemical sensor as a sensing platform has been proven effective in detecting SARS-CoV-2 viral infection.[8,9] The electrochemical sensor is the best alternative to biochemical analysis and immunoassays in medical diagnostics owing to low-cost instrumentation, portability, rapidity, precision, and sensitivity.[10–12] As such, Alafeef *et al.* employed the integration of thiol-modified antisense oligonucleotide probes, which are single-stranded DNA (ssDNA) sequence probes with capped gold nanoparticles (AuNPs) that are specific and selective for the nucleocapsid (N) gene for COVID-19 detection.[13]

Hence, to mitigate the limitations of real-time RT-PCR, an electrochemical sensor for clinical COVID-19 detection following the guidelines formulated by WHO is an ideal diagnostic tool in a resource-limited setting.[14,15] Therefore, a miniaturized electroanalytical system was implemented with Au-nanoparticle-modified screen-printed carbon electrodes as these sensors require only microliters of samples.[16] Malecka *et al.* used a screen-printed gold electrode (SPGE) for the electrochemical detection of specific DNA and RNA sequences derived from avian influenza virus (AIV H5N1).[15] In their study, a monolayer of thiolated DNA probe (SH-NC_3) and 6-mercaptohexanol (MCH) was deposited onto the SPGE surfaces incorporated with a sensitive ion-channel mimetic miniaturized genosensor.[15] The critical challenges would be in the mass production of SH-NC_3 and MCH via deposition on the SPGE surface and direct RNA sequencing without a reverse transcription from RNA to DNA.

The RT-LAMP assay coupled with Au/SPCE can be one of the unified platforms for the Internet of Things (IoT). The electrochemical signals can be read and recognized through information-sensing devices controllable through IoT. The RT-LAMP method involves six target sequences simultaneously recognized by separate definite primers in the same reaction; thus, the

method has high detection specificity and sensitivity.[17,18] Moreover, the advantages of the RT-LAMP assay for SARS-CoV-2 nucleic acid amplification include a quick and reliable detection as it can detect small amounts of DNA or RNA templates within an hour. Moreover, RT-LAMP requires inexpensive instruments and environment-friendly reagents and promotes point-of-care testing (POCT).[19,20] Ramírez-Chavarría *et al.* successfully developed a technique for the genetic amplification of the COVID-19 genome by RT-LAMP integrated with electrical impedance spectroscopy (EIS) analysis using time-constant domain spectroscopy (TCDS).[21] The TCDS served to assess the RT-LAMP products and classify the positive and negative COVID-19 samples.[21] Interestingly, a rapid multiplexed ultrasensitive sample-to-answer loop-mediated isothermal amplification chip for simple LED-driven photothermal amplification was developed for the detection of SARS-CoV-2 and an influenza virus concurrently. This chip is highly sensitive with a limit of detection (LOD) of 0.5 copies μl^{-1} for SARS-CoV-2 detection and could identify different genes within an assay in the presence of many other viruses.[22] Zhang *et al.* enabled the identification of purified COVID-19 viral RNA using RT-LAMP assay by colorimetric detection without IoT embodiment.[23,24] In the scenario of the COVID-19 pandemic, IoT could store a vast amount of patient data, provide personalized medicine, and retrieve test results via smartphone applications, which can be accessed by not only healthcare providers but also individuals.[24]

Here, the clinical performance of the RT-LAMP assay using COVID-19 nasopharyngeal swab samples on the AuNP/SPCE using DPV was evaluated. First, a bioinformatics study on the N gene region of the SARS-CoV-2 genome structure was conducted to find a specific DNA sequence as the RT-LAMP primer. The RT-LAMP primer was then used in the RT-LAMP mix reagent for the amplification process. The amplification product was validated using gel electrophoresis. AuNP/SPCE was used as a sensing platform with 5 mM $K_4[Fe(CN)_6]$ as the background electrolyte. Approximately 4 μL of the RT-LAMP products was dropped on AuNP/SPCE and DPV was conducted, which resulted in distinct signal outputs of the blank (5 mM $K_4[Fe(CN)_6]$, positive control, negative control, and positive and negative samples. The results of the clinical assays using the developed electrochemical sensor were statistically compared with those obtained by the real-time RT-PCR (gold standard) endorsed by the Institute for Medical Research, National Institute of Health, and Ministry of Health (MOH), Malaysia.

2. Data, Materials, and Methods

2.1 Ethical approval

Ethical approval was granted by the UiTM Research Ethics Committee (REC) with referral number REC/03/2022 (PG/MR/51) and Medical Research Ethics Committee (MREC), MOH, with referral number NMRR ID-22-006675-CFP; Protocol ID: 14022022.

2.2 Reagents and materials

The COVID-19 RNA extraction kit used in this research was the QIAamp Viral RNA Mini Kit (Qiagen, German) with 99% ethanol obtained from Thermo Fisher Scientific Inc. The

Real-Q 2019-nCoV detection kit purchased from BioSewoom Inc. (Seoul, Republic of Korea) was the COVID-19 detection kit used for the real-time RT-PCR procedure. WarmStart® Colorimetric 2X Master Mix with UDG (New England Biolabs Inc., Massachusetts, USA) was used as the RT-LAMP reagent kit. The ISO 13485-certified SPCE modified with AuNP was obtained from Metrohm DropSens, Spain. Potassium ferrocyanide ($K_4[Fe(CN)_6]$) and potassium chloride (KCl) were purchased from Sigma Aldrich, USA. Sulphuric acid (H_2SO_4) was obtained from R&M Chemicals, Malaysia.

2.3 Clinical COVID-19 samples

The nasopharyngeal swabs of clinical COVID-19 samples were placed in viral transport media (VTM) upon collection (n = 148) from the COVID-19 laboratory, Institute for Medical Research, National Institute of Health, Setia Alam, Selangor, Malaysia. The COVID-19 samples were transported in an ice box for a maximum of 72 h at 2–8 ℃ after collection. The RNA extraction and real-time RT-PCR procedure were conducted immediately after the collection.

2.4 Inactivation of COVID-19 samples

The COVID-19 samples were heat-inactivated at 65 ℃ for 1 h in a GFL-70 Blast Dry Oven at the COVID-19 laboratory, Institute for Medical Research, National Institute of Health, Setia Alam, Selangor, Malaysia.

2.5 Extraction of COVID-19 RNA

Approximately 140 µl of COVID-19 RNA from the nasopharyngeal swab samples was extracted using the QIAamp Viral RNA Mini Kit (Qiagen). The samples were extracted following a standard procedure guided by the manufacturer and approved by the Institute for Medical Research, National Institute of Health, Malaysia. The extraction procedure involves a series of incubation and filtration steps with several types of buffer such as lysis, wash, and elution buffers to obtain the extracted RNA of COVID-19.

2.6 COVID-19 RT-LAMP assay development

The WarmStart® colorimetric assay was conducted using a specifically selected sequence of primers targeting the N gene of SARS-CoV-2. The RT-LAMP assay was performed in 23.0 µl of reaction mixture consisting of 12.5 µl of WarmStart® colorimetric 2× master mix with UDG (NEB, Ipswich, United Kingdom), 2.5 µl of 10X primer mix, 2.5 µl of 4 mM guanidine hydrochloride solution, and 5.5 µl of nuclease-free molecular-biology-grade water incubated at 65 ℃ in an incubator (GFL-70 Blast Dry Oven) for 35–40 min.

2.6.1 RT-LAMP target selection and specific primer design

The conserved sequence of the N gene was determined on the basis of the multiple alignment of the available completed SARS-CoV-2 sequences obtained from the GenBank database using the NCBI Multiple Alignment tools and Jalview software. The RT-LAMP target region was selected on the basis of the sequences that showed more than 98% nucleotide similarities. For *in silico* specificity analysis, the homology of the target region sequence was compared with that of the N gene sequence of several other related coronaviruses and high-priority pathogens using Nucleotide BLAST (BLASTn). The result for *in silico* specificity was obtained on the basis of local and global pairwise alignment.

2.6.2 Colorimetric RT-LAMP product

Approximately 2 µl of extracted RNA of COVID-19 samples was dropped into 23.0 µl of RT-LAMP reagent. The samples were incubated at 65 ℃ in an incubator (GFL-70 Blast Dry Oven) for 35–40 min. The RT-LAMP product also included positive and negative controls. The positive control (PC) consisted of 2 µl of a plasmid containing the target sequence of SARS-CoV-2. The negative control (NC) consisted of only RT-LAMP reagents without any amplification templates. The color change (pink to yellow) indicates positive amplification, whereas the unchanged color (remained pink) indicates negative amplification. The product of RT-LAMP amplification was further analyzed by running the products by 2% agarose gel electrophoresis for 40 min (4000 mA, 90 V) and visualized under blue light. The presence of a ladder pattern band on lane (L) in the gel electrophoresis readout indicated positive amplification. The LOD of the RT-LAMP assay was obtained by determining the lowest number of plasmid copies (1.6, 0.8, 0.4, or 0.2) per microliter that caused the color change from pink to yellow.

2.7 Real-time RT-PCR for COVID-19 detection

The extracted RNA of COVID-19 samples was subjected to real-time RT-PCR, which was performed using the Real-Q 2019-nCoV detection kit (BioSewoom, Seoul, Republic of Korea) with the CFX96 real-time PCR detection system (Bio-Rad Laboratory, Inc., California, U.S.A.) as approved by the Institute for Medical Research, National Institute of Health, and MOH, Malaysia. The reaction mixture or master mix is composed of 3.50 µl of RNase-free water (RFW), 12.50 µl of 2X PCR reaction mixture, 3.00 µl of nCoV primer and probe mix, and 1.00 µl of RT-PCR enzyme with 5.0 µl of template or sample. The positive control used in this study was provided by the manufacturer, whereas for the negative control, no reagent was added to the master mix. The real-time RT-PCR was also carried out under the following conditions: reverse transcription at 50 ℃ for 30 min, pre-denaturation at 95 ℃ for 15 min, denaturation at 95 ℃ for 15 s, and extension at 62 ℃ for 45 s in 40 cycles. The results of the real-time RT-PCR were analyzed by reading the threshold value (C_T), which was the replication cycle required to yield the fluorescent signal. C_T is the cycle during which the fluorescent signal exceeded the background level and crossed the threshold. The cut-off value for the real-time RT-PCR was

standardized following the guidelines provided by the Institute for Medical Research and MOH, Malaysia. A C_T value of less than 38 indicated that COVID-19 was detected (a positive reading), whereas a C_T value of more than 38 indicated that COVID-19 was not detected (a negative reading).

2.8 Fabrication of gold nanoparticles on screen-printed carbon electrode

A mixture of 10 mM gold (III) chloride trihydrate ($HAuCl_4{\cdot}3H_2O$) and 1 M sulphuric acid (H_2SO_4) was prepared as the deposition solution. The electrodeposition of AuNP on the SPCE was carried out using a three-electrode system with the built-in printed electrode in the SPCE serving as the reference electrode (Ag) and carbon (C) serving as the counter electrode. The SPCE was submerged in 10 mM $HAuCl_4{\cdot}3H_2O$ + 1 M H_2SO_4, and the cyclic voltammetry sweep was performed for 50 cycles (15 min) from +0.5 to −0.6 V at room temperature. The resulting AuNP/SPCE was then rinsed with deionized water, dried using a nitrogen stream, and stored in a desiccator for future use.

2.9 Clinical COVID-19 assay on AuNP/SPCE using DPV

A 5 mM $K_4[Fe(CN)_6]$ solution containing 0.1 mM KCl and 5 mM ferrocyanide ($[Fe(CN)_6]^{4-}$ was used not only as an electrochemical label but also as a blank solution. Approximately 4 µl of the COVID-19 samples (RT-LAMP product) [N = 148; (n = 74 positive samples (PS) and n = 74 negative samples (NS)] was dispensed onto the AuNP/SPCE (gold working electrode), followed by 100 µl of $K_4[Fe(CN)_6]$ background electrolyte. An incubation time of 5 min (optimal) was employed prior to DPV electroanalysis. The DPV was conducted by scanning the potential range from −0.2 to +0.6 V, the pulse amplitude of 0.002 V, the pulse period (t_{pulse}) of 50 ms, and the scan rate of 0.025 Vs^{-1}. The resulting signals of the samples were analyzed using a portable custom-built potentiostat (NACOTS,UiTM, Malaysia) connected to the sensor through a USB port for the signal readout. The DPV response signals of the peak current (I_p) (µA) for all the samples were obtained. The ΔI (µA) for the COVID-19 samples was obtained from the differences between the I_p of the blank and that of the COVID-19 samples.

$$\Delta I = I_{p(BLANK)} - I_{p(POSITIVE\ SAMPLES)} \tag{1}$$

$$\Delta I = I_{p(BLANK)} - I_{p(NEGATIVE\ SAMPLES)} \tag{2}$$

2.10 Receiver operating characteristic (ROC) curve analysis

The ROC curve analysis was applied to investigate the cut-off ΔI (µA) values for the developed sensor between the positive and negative clinical COVID-19 samples. The ROC curve is useful for assessing the effectiveness of the diagnostic procedure. The curve is interpreted as the test's sensitivity (the y-coordinate) against the test's 1-specificity (the x-coordinate). The value with the highest Youden's index and adequate sensitivity based on the ROC analysis was chosen as the ideal cut-off value for further analysis.

2.11 Statistical analysis

The significant difference between positive and negative clinical samples was analyzed using Student's *t*-test and validated on GraphPad Prism version 9 (GraphPad Software Inc., USA). At a 95% confidence interval (CI), the results were not significant when the two-sided *p*-value was more than 0.05 ($p > 0.05$). The 148 nasopharyngeal swab samples [$n = 74$ (PS) and $n = 74$ (NS)] with 95% confidence or 95% reliability were tested on AuNP/SPCE and clinically compared with the real-time RT-PCR test. The clinical sensitivity, which is defined as the number of abnormal conditions, and the specificity, which is defined as the number of normal conditions, were analyzed.[25]

3. Results and Discussion

3.1 Identification of COVID-19 samples by RT-LAMP assay and CFX96 real-time PCR detection system

The extracted RNAs from COVID-19 samples ($N = 148$) were subjected to the RT-LAMP assay and produced the following results: 53 samples ($n = 53$) showed color changes, whereas the other samples ($n = 95$) remained pink. The results obtained indicate that 52 samples were true positive, 22 samples were false negative, 73 samples were true negative, and a sample was false positive. The results of the colorimetric RT-LAMP indicated that the PS showed a change in color from pink to yellow, whereas the NS showed no change in color (remained pink) after heat incubation at 65 °C for 35–40 min as shown in Fig. 1. However, some of the PS remained pink

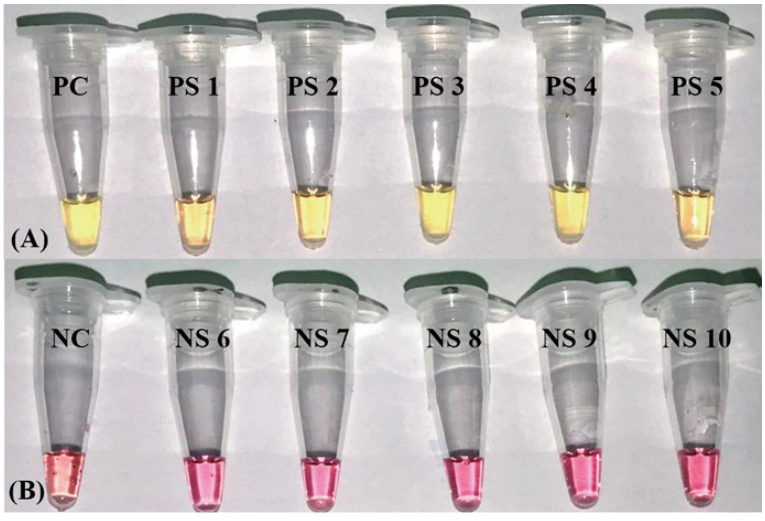

Fig. 1. (Color online) Typical detection of COVID-19 by reverse transcription loop-mediated isothermal amplification (RT-LAMP) with the end product of color changes based on colorimetric readout. (A) Positive control (PC) and positive samples (PS 1 to PS 5) or amplified RT-LAMP products that changed color from pink to yellow. (B) Negative control (NC) and negative samples (NS 6 to NS 10) of RT-LAMP products that showed no change in color or remained pink.

under 30 min of incubation at 65 °C because the C_T values of RT-PCR ranged from 30 to 38 (C_T > 30–38). The detected COVID-19 samples appeared orange, which was classified as an indeterminate viral load. This classification is due to false positives or false negatives from visual observation.[26,27] Hence, the development of a COVID-19 diagnostic sensor assay as such is relevant for viral detection because color changes from calorimetric RT-LAMP assays might lead to the misinterpretation of clinical results. The positive and negative controls were also run to indicate the reliability of the test.

In principle, the color change in the RT-LAMP assay from pink to yellow is attributable to phenol red as a pH indicator, which allowed a clear visual detection to distinguish between NS and PS. The color changes from pink to yellow at pH 6.8 because the reaction mix was bound with phenol red. The production of protons and the decrease in pH occurred because of the extensive RNA polymerase activity in the RT-LAMP reaction. Throughout the amplification by RT-LAMP, the protons produced caused the pH to change from neutral to acidic. Next, dNTPs were integrated by DNA polymerase into the growing DNA chain. Pyrophosphate compounds and hydrogen ions were emitted as by-products of this chemical reaction. The emission of hydrogen ions was directly proportional to the quantity of newly integrated dNTPs, thus releasing a large amount of hydrogen ions. The formation of hydrogen ions during RT-LAMP substantially and promptly shifted the pH across the threshold of phenol red from pH 8.5 to pH 6.8. The positive amplifications can be seen clearly owing to the increase in the amount of H^+ ions resulting from DNA amplification in the RT-LAMP master mix.[28]

The RT-LAMP products were further visualized by agarose gel electrophoresis to determine the presence of amplified products for PS and to detect any contamination in the NS. Figure 2

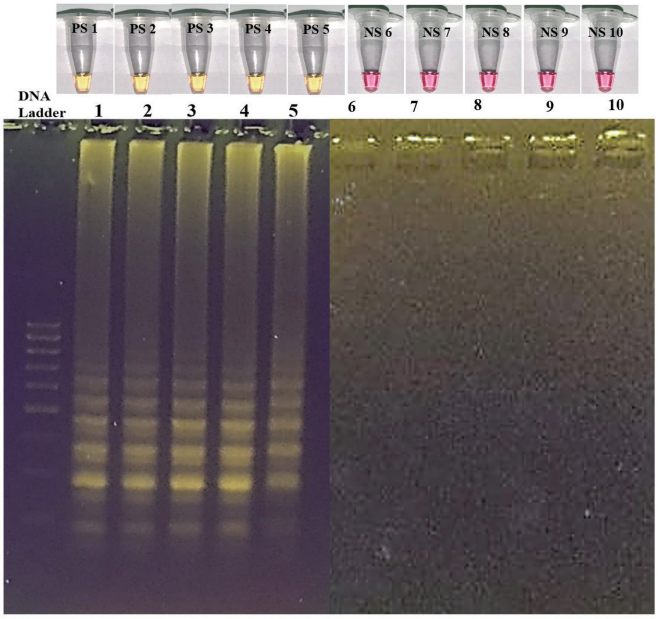

Fig. 2. (Color online) Agarose gel electrophoresis of typical loop-mediated isothermal amplification (RT-LAMP) products for PS from lanes 1 to 5 and NS from lanes 6 to 10.

shows the presence of ladder pattern bands for the amplified products of PS in lanes 1 to 5, whereas ladder pattern bands are absent for the NS in lanes 6 to 10. The absence of ladder pattern bands for samples indicates that there was no contamination or any reaction.

From the real-time RT-PCR, the results obtained were 74 PS and 74 NS. From these results, the PS showed C_T values of less than 38 ($C_T < 38$), whereas the NS presented C_T values of more than 38 ($C_T > 38$). The C_T values for three gene must be determined to indicate that the samples were either positive or negative. Three types of genes were considered in the procedure, namely, RNA-dependent RNA polymerase (RdRp), envelope protein (E), and ribonuclease (RNP) genes or internal control (IC). The first-line screening test was based on an E-gene assay followed by a confirmatory assay using the RdRp gene, since real-time RT-PCR assays targeting the RdRp gene had the greatest analytical sensitivity.[29] The RNP gene indicated the presence of human genes or showed a good sampling procedure by nasopharyngeal swab and proper nucleic acid extraction.[2] Hence, the values of PS were calculated as the C_T values of the E, RdRp, and RNP genes to be less than 38 ($C_T < 38$). The values of the NS were more than 38 ($C_T > 38$) for the RdRp and E genes, whereas IC presented C_T values of less than 38 ($C_T < 38$) to indicate the appropriate method of nasopharyngeal swab sampling.[30]

As mentioned, the target site for the developed RT-LAMP assay was located at the N gene. According to CDC, it is recommended to utilize two primer-probe sets targeting the N gene (N1 and N2) to achieve a more sensitive and specific detection of COVID-19.[2] Furthermore, the infected cell was found to have many coronavirus N proteins since it has been postulated that these proteins play roles in virus replication, transcription, and translation.[30] Fifty-three COVID-19 samples for RT-LAMP showed a color change (pink to yellow), whereas the other samples showed no change in color (remained pink). The results of both methods showed equivalent qualitative values. The results of RT-LAMP and real-time RT-PCR are shown in Supplementary Table 1.

Table 1
In silico cross-reactivity of RT-LAMP primer with other viruses.

RT-LAMP Target Region	Organism	Gene	Searches	
			Global (%)	Local (%)
N gene of SARS-CoV-2	Human Coronavirus 229E (NC_002645.1)	Nucleocapsid	15.0	17.6
	Human Coronavirus OC43 (AY391777.1)	Nucleocapsid	13.0	12.2
	Human Coronavirus HKU1 (NC_006577.2)	Nucleocapsid	14.0	13.1
	Human Coronavirus NL63 (NC_005831)	Nucleocapsid	16.0	16.6
	SARS-Coronavirus (NC_004718.3)	Nucleocapsid	14.0	94.9
	MERS-Coronavirus (KT006149.2)	Nucleocapsid	14.0	16.8
	Human Adenovirus (DQ315364.2)	Nucleocapsid	13.0	13.2
	Influenza A (NC_007369.1)	Nucleocapsid	12.0	13.2
	Influenza B (NC_002208.1)	Nucleocapsid	11.0	12.4
	Human Parainfluenza 1 (NC_003461.1)	Nucleocapsid	12.0	10.8
	Human Parainfluenza 2 (NC_003443.1)	Nucleocapsid	11.0	11.8
	Human Parainfluenza 3 (NC_001796.2)	Nucleocapsid	12.0	11.7
	Human Parainfluenza 4 (NC_021928.1)	Nucleocapsid	11.0	10.7

3.2 *In silico* cross-reactivity analysis of RT-LAMP assay

The cross-reactivity of the RT-LAMP target region of the N gene was further tested with other coronaviruses such as the influenza virus and adenovirus. Table 1 shows that the RT-LAMP primer does not indicate a cross-reactivity with other N genes of other viruses. Thus, the developed RT-LAMP primer was unique and specific to the N gene of COVID-19.

In contrast, the RT-LAMP could also be used with multiplex amplifications with the development of a high-fidelity DNA polymerase-mediated probe (HFman probe) in detecting other target variants of COVID-19 that are aligned with the recent emerging COVID-19 mutants. This system could simultaneously detect open reading frame (ORF) and E genes in an assay.[31] In addition, there are also other studies with three different primer sets of RT-LAMP showing that the multiplex isothermal amplification could detect the RdRP, E, and N genes of SARS CoV-2 in a single tube.[32]

3.3 Morphology and electrochemical performance of AuNP/SPCE

FESEM analysis was conducted to study the morphology of the electrodeposited AuNP/SPCE and unmodified SPCE. It can be observed from the FESEM images shown in Fig. 3 that the AuNPs obtained were quasi-spherical with a faceted shape and a diameter of ±500 nm. After modification, the SPCE surface is fully covered with AuNPs as shown in Figs. 3(a) and 3(b). The agglomeration of AuNPs can be observed in Fig. 3(b) owing to the aggregated growth of two neighboring AuNPs or amorphous atom clusters.[33]

The deposition of AuNPs onto the SPCE was performed using cyclic voltammetry with a potential range from +0.5 to 0 V for 90 cycles at a scan rate of 50 mVs^{-1}. The deposition process typically takes up to 30 min. As the number of cycles increased, the reduction potential shifted

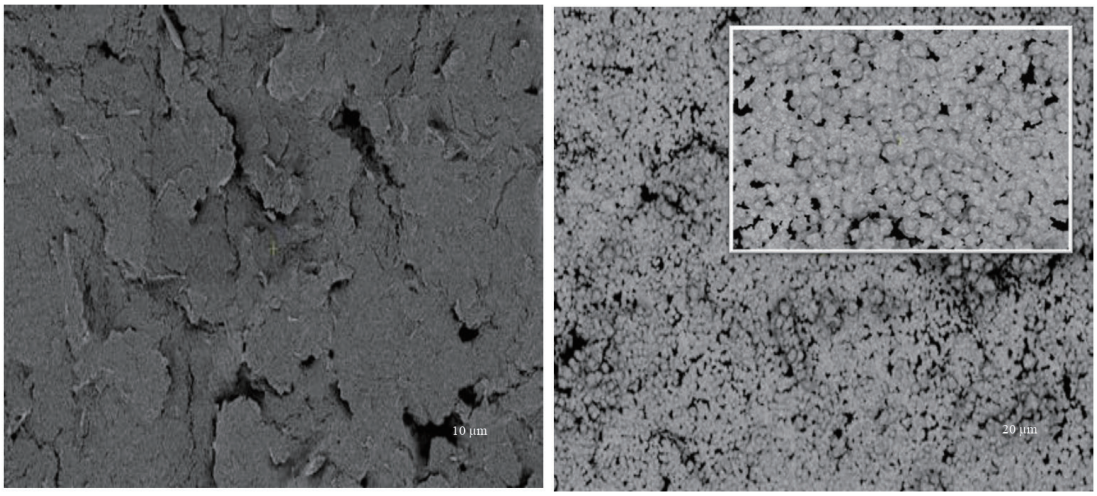

(a) (b)

Fig. 3. FESEM images of (a) unmodified SPCE and (b) AuNP/SPCE at 5 K magnification. The inset in (b) shows 10 K magnification.

to a more positive value, indicating the successful electrodepositions of AuNPs from the previous scans as shown in Fig. 4. This cathodic peak shifting is consistent with the finding by Zakaria *et al.*[33] The performance characteristics of both the AuNP/SPCE and the unmodified SPCE were evaluated using cyclic voltammetry in a solution containing 10 mM $K_4[Fe(CN)_6]$ and 0.1 M KNO_3. The results shown in Fig. 5 indicate that the AuNP/SPCE surface had the highest redox current response of ferrocyanide ions when compared with the unmodified SPCE. The observed increase in redox current response can be attributed to the enhanced electrical conductivity of the SPCE surface resulting from the good electrical contact of the deposited AuNPs. This increased conductivity allows for a more efficient electron transfer during the

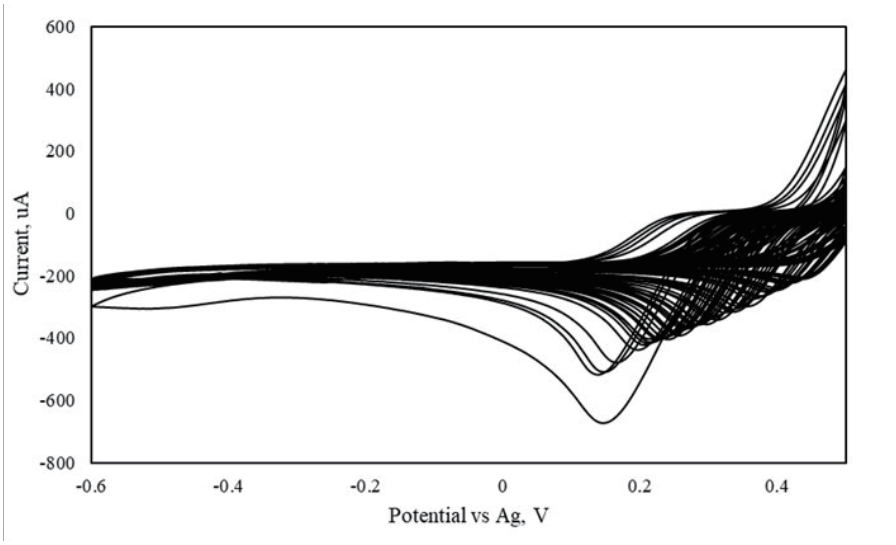

Fig. 4. Cyclic voltammograms of electrodeposition of AuNP/SPCE in 10 mM $HAuCl_4$ in 0.1 M H_2SO_4.

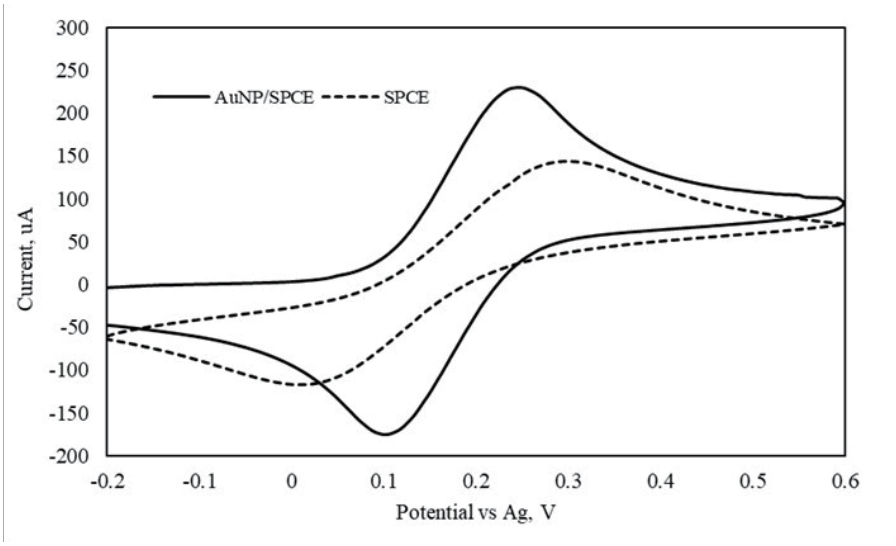

Fig. 5. Cyclic voltammograms of electrochemical performance characteristics of AuNP/SPCE and unmodified SPCE in 10 mM $K_4Fe(CN)_6$ + 0.1 M KNO_3.

redox process, which leads to a higher redox current response. Therefore, the AuNP/SPCE sensor is more efficient than the unmodified SPCE sensor in detecting analytes at lower concentrations.

3.4 Evaluation of COVID-19 samples by COVID-19 diagnostic assay

The RT-LAMP products were dropped on the electrodes and run with the sensor by the DPV method. As shown in Fig. 6(a), there were differences in the electrochemical and morphological profiles of the AuNP/SPCE with PS and NS. The peak height (I_p) (μA) for the blank is larger than those for NS and PS. The blocking effect due to the presence of DNA at the electrode caused a decrease in the oxidation peak current (I_p) (μA) of the ferrocyanide ion.[7] The value of ΔI for all COVID-19 samples was calculated using Eqs. (1) and (2) and the results are shown in Supplementary Table 1. Figure 6(b) shows the mean difference (ΔI) (μA) in PS value, which showed a higher ΔI response than that in NS value. From the results of the statistical analysis using Student's *t*-test, at a 95% CI, a significant difference was observed between the PS and NS ($p < 0.0001$) responses.

3.5 Cut-off point for COVID-19 sensor

The cut-off ΔI values between normal and abnormal conditions were analyzed using the ROC curve shown in Fig. 7. On the basis of the analysis results, we determined that the ideal cut-off value with the highest Youden's index is more than 0.94 μA. The area under the curve was 0.905 ($p < 0.0001$) with the maximum Youden's index at 0.65, corresponding to a critical cut-off value of 0.94 μA. The clinical sensitivity of 79.7% and the specificity of 85.1% (Table 2) were obtained.

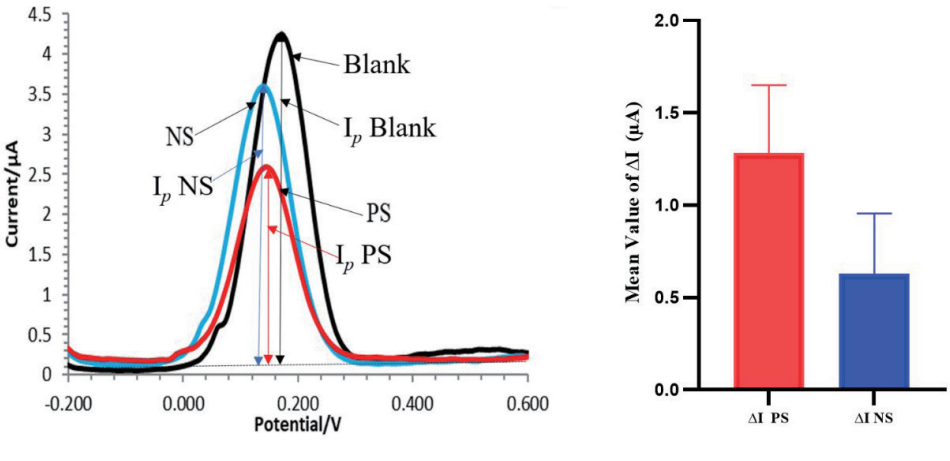

(a) (b)

Fig. 6. (Color online) (a) DPV using 5 mM $K_4[Fe(CN)_6]$ as blank, PS, and NS with amplitude modulation: potential range from −0.2 to +0.6 V, pulse amplitude of 0.002 V, pulse period (t_{pulse}) of 50 ms, and scan rate of 0.025 Vs^{-1}. (b) Mean values and standard deviations of PS and NS.

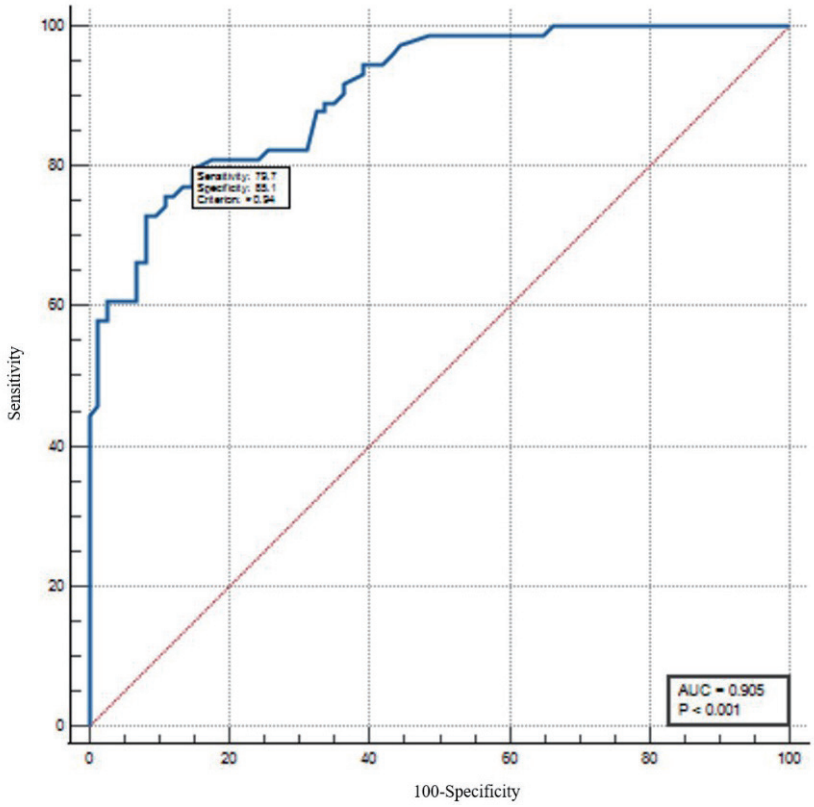

Fig. 7. (Color online) ROC curve of COVID-19 samples.

Table 2
Area under the curve and diagnostic performance of the test.

ROC curve area	Cut-off value (μA)	Youden's index	Sensitivity (%)	Specificity (%)	*p*-value
0.905	>0.94	0.65	79.7	85.1	<0.0001

3.6 Reliability of sensor performance compared with real-time RT-PCR

Real-time RT-PCR is demanding as it is laboratory-based and requires highly trained personnel to perform. These inconveniences cause difficulties for healthcare providers to perform the tests. However, compared with real-time RT-PCR, the electrochemical sensor tested in this study was found to be more reliable in detecting COVID-19. The sensor can be utilized as a POCT instrument in different sites such as stadiums and schools or in any events. The longer time required to run the samples using real-time RT-PCR may contribute to delays in delivering the results, which could cause fatalities due to late treatment and increase the number of cases due to an increased possibility that the COVID-19 virus has been more widely spread. Furthermore, the cost of utilizing the electrochemical sensor is not as high as the cost of real-time RT-PCR. The instrumentation cost of electrochemical analysis is about US$ 1000 compared

with RT-PCR that costs US$ 30000. Hence, there are price reduction of 25% per test and 96% for the instrument. Therefore, the price reduction can helps the government in controlling the budget and sustain the economy. Table 3 shows the comparison between real-time RT-PCR and the electrochemical sensor. The significant difference in performance between both instruments or methods was evaluated using GraphPad Prism Version 9 and Student's *t*-test at a 95% CI. The mean difference in the bar graph with standard deviation showed no significant difference between real-time RT-PCR and the sensor as the *p*-value is 0.7729 ($p \geq 0.05$) as shown in Fig. 8. The data from real-time RT-PCR and the COVID-19 sensor are tabulated in Supplementary Table 1. Table 4 shows the diversities of sensing platforms for COVID-19 detection, namely, electrochemical immunosensors, paper-based biosensors, and microfluidic multiplexed polymer-based biosensors that are in accordance with specific medical and economic situations. Ultimately, this developed detection method is much more suitable for SARS-CoV-2 RNA sensing in a resource-limited setting.

Table 3
Comparison between real-time RT-PCR and electrochemical sensor.

Components	Real-time RT-PCR	Electrochemical Sensor
Portability	Not portable	Portable
Analysis time	~2 h	~30 s
Turnaround time (TAT)	~6 h	~1 to 2 h
Cost per test	RM70.68	RM53.03
Limit of detection (LOD)	3.125 copies μl^{-1}	0.4 copies μl^{-1}

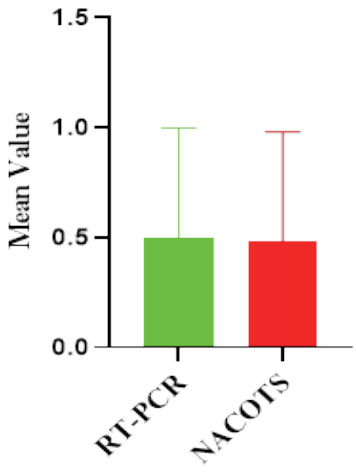

Fig. 8. (Color online) Mean difference with standard deviation between real-time RT-PCR and COVID-19 sensor.

Table 4
Comparison of three sensing platforms for COVID-19 detection.

Sensing Platform	Remarks	References
Screen-printed carbon electrodes (SPCEs) with electrodeposited gold nanostructures (AuNS) modified with SARS-CoV-2 spike proteins (rSpike) for the detection of specific antibodies	The LOD claimed by the authors for the DPV signal was 0.14 nM, and it was suggested to be applied to COVID-19 patients before and after vaccination as the specificity test was evaluated and found to show nonspecificity towards anti-rSpike antibodies.	Drobysh *et al*., 2022[34]
Lateral flow immunoassay (LFIA)-based biosensor: production of antibodies and single-chain variable fragment (scFv)-crystallizable fragment (Fc) fusion proteins (scFv-Fcs) by phage display technology for the specific detection of SARS-CoV-2 nucleocapsid protein (NP).	The biosensor can detect COVID-19 within 20 min with no cross-reactivity with other coronaviruses such as SARS-CoV and MERS-CoV.	Kim *et al*., 2021[35]
Microfluidic multiplexed polymer-based biosensor in combination with CRISPR/Cas-powered assays. Omicron variants of envelope (E) and RNA-dependent RNA polymerase (RdRp) genes were detected by using Leptotrichia buccalis (Lbu)Cas13a.	The LOD for the E gene was 2000 copies μl^{-1} and that for the RdRp gene was 7520 copies µl–1. The time taken to process the sample until the result was obtained was approximately 30 min.	Johnston *et al*., 2022[36]
Detection of nucleocapsid (N) gene using a specifically designed primer sequence for RT-LAMP and dropped on AuNP/SPCE and portable potentiostat	The LOD for the RT-LAMP assay was 0.4 copies μl^{-1} with an analysis time of 30 s and a TAT of approximately 1 h. The clinical sensitivity and specificity were 79.7% and 85.1%, respectively.	This work

4. Conclusions

This study revealed that the clinical results for COVID-19 samples (N = 148) using the RT-LAMP assay were comparable to those obtained using real-time RT-PCR. The sensor platform used in this study was AuNP/SPCE, and the morphological surface was proven by FESEM to have gold nanoparticles. The RT-LAMP products were analyzed on Au/SPCE with DPV response using a custom-built portable potentiostat. The PS showed a lower (ΔI) mean than the NS. The PPA value of the sensor was 100%. The ΔI values of the PS and NS were significantly different with a p-value of 0.0001 ($p < 0.05$) at a 95% CI on Student's t-test. The real-time RT-PCR instrumentation and analysis were more tedious, laborious, and costly than the RT-LAMP electroanalytical method, which was convenient, inexpensive, and portable. The LOD for the RT-LAMP assay was 0.4 copies μl^{-1}, whereas that for the Biosewoom Real-Q 2019-nCoV commercial detection kit was 3.125 copies μl^{-1}. However, the colorimetric result from the RT-LAMP alone could lead to insensitivity in evaluating the color changes as the reading would be affected by surrounding light due to the spectral composition of the light source. A color-blind person might also contribute to the false positive and negative reading of the RT-LAMP product. Hence, DPV enables the integration with the IoT system for better data collection, storage, and analysis that enhance the decision making in outbreak management.

Acknowledgments

This research project was funded by the UiTM Internal Grant (600-RMC/KEPU 5/3 (157/2021) and the Ministry of Science, Technology, and Innovation (MOSTI) under the Combating COVID-19 Fund (project number: CV 02211032) grants.

References

1 World Health Organization: https://apps.who.int/iris/handle/10665/331686%0ADescription (accessed January 2023).
2 Centers for Diseases Control and Prevention (CDC): https://www.fda.gov/media/134922/download (accessed November 2022).
3 X. Lizhou, L. Danyang, R. Sami, L. Yanbin, and K. Norbert: Biosens. Bioelectron. **170** (2020) 2. https://doi.org/10.1016/j.bios.2020.112673
4 N. Chen, M. Zhou, X. Dong, J. Qu, F. Gong, Y. Han, Y. Qiu, J. Wang, Y. Liu, Y. Wei, J. Xia, T. Yu, X. Zhang, and L. Zhang: Lancet **395** (2020) 508. https://doi.org/10.1016/S0140-6736(20)30211-7
5 C. Huang, Y. Wang, L. Xingwang, L. Ren, J. Zhao, Y. Hu, L. Zhang, G. Fan, J. Xu, X. Gu, Z. Cheng, T. Yu, J. Xia, Y. Wei, W. Wu, X. Xie, W. Yin, H. Li, M. Liu, Y. Xiao, H. Gao, L. Guo, J. Xie, G. Wang, R. Jiang, Z. Gao, Q. Jin, J. Wang, and B. Cao: Lancet. **395** (2020) 500. https://doi.org/10.1016/S0140-6736(20)30183-5
6 S. Monteil, A. J. Casson and S. T. Jones: PloS One. **16** (2021) 1. http://dx.doi.org/10.1371/journal.pone.0258002
7 A. C. R. Moço, P. H. Guedes, J. M. R. Flauzino, S. Silva, J. G. Vieira, A. C.Castro, E. V. R. Gomes, F. M. Tolentino, M. M. C. N. Soares, J. M. Madurro, and A. G. Brito-Madurro: Electroanalysis. **31** (2019) 1. https://doi.org/10.1002/elan.201900068
8 L. F. D. Lima, A. L. Ferreira, M. D. T. Torres, W. R. D. Araujo, and C. D. L Fuente-Nunez: Proc. National Academy of Sciences of the United States of America (2021) 1–9.
9 S. Tripathy and S. G. Singh: Trans. Indian Natl. Acad. Eng. **5** (2020) 205. https://doi.org/10.1007/s41403-020-00103-z
10 Y. Lee, J. Choi, H. K. Han, S. Park, S. Y. Park, C. Park, C. Baek, T. Lee, and J. Min: Sens. Actuators, B **326** (2021) 2. https://doi.org/10.1016/j.snb.2020.128677
11 E. Zeynaloo, E. Zahran, Y. P. Yang, E. Dikici, T. Head, L. G. Bachas, and S. Daunert: Biosens. Bioelectron. **200** (2021) 2. https://doi.org/10.1016/j.bios.2021.113861
12 S. Jain, M. Nehra, R. Kumar, N. Dilbaghi, T. Y. Hu, S. Kumar, A. Kaushik, and C. Z. Li: Biosens. Bioelectron. **179** (2021) 4. https://doi.org/10.1016/j.bios.2021.113074
13 M. Alafeef, K. Dighe, P. Moitra, and D. Pan. Rapid: ACS Nano. **14** (2020) 17028. https://doi.org/10.1016/j.mattod.2022.11.001
14 G. Rosati, A. Idili, C. Parolo, C. Fuentes-Chust, E. Calucho, L. Hu, C. D. C. C. E Silva, L. Rivas, E.P. Nguyen, J. F. Bergua, R. Alvarez-Diduk, J. Munoz, C. Junot, O. Penon, D. Monferrer, E. Delamarche, and A. Merkoci: ACS Nano. **15** (2021). https://doi.org/10.1021/acsnano.1c06839
15 K. Malecka, A. Stachyra, A. Góra-sochacka, A. Sirko, W. Zagórski-ostoja, H. Radecka, and J. Radecki: Sens. Actuators, B **224** (2015) 290. http://dx.doi.org/10.1016/j.snb.2015.10.044
16 A. C. Power and A. Morri: Electrochemistry (IntechOpen, Rijeka, 2013) Chap. 7.
17 T. Notomi, H. Okayama, H. Masubuchi, T. Yonekawa, K. Watanabe, N. Amino, and T. Hase: Nucleic Acids Res. Spec. Publ. **28** (2000) 63. https://doi.org/10.1093/nar/28.12.e63
18 X. Huang, G. Tang, N. Ismail, and X Wang: EBioMedicine. **75** (2022) 103736. https://doi.org/10.1016/j.ebiom.2021.103736
19 M. Shen, Y. Zhou, Ye J, A. A. A. AL-Maskri, Y. Kang, S. Zeng, and S. Cai: J. Pharm. Anal. **10** (2020) 97. https://doi.org/10.1016/j.jpha.2020.02.010
20 A. Basu, T. Zinger, K. Inglima, K. M. Woo, O. Atie, L. Yurasits, B. See, and M. E. Aguero-Rosenfeld: J. Clin. Microbiol. **58** (2020) 2. https://doi.org/10.1128/jcm.01136-20
21 R. G. Ramírez-Chavarría, E. Castillo-Villanueva, B. E. Alvarez-Serna, J. Carrillo-Reyes, L. Torres, R. M. Ramírez-Zamora, G. Buitron, and L. Alvarez-Icaza: Chemosensors. **11** (2023) 2. https://doi.org/10.3390/chemosensors11040230
22 M. Song, S. Hong, and L. P. Lee: Adv. Mater. **35** (2023) 2. https://doi.org/10.1002/adma.202207138
23 Y. Zhang, N. Odiwuor, J. Xiong, L. Sun, R. O. Nyaruaba, H. Wei, and Na. Tanner: MedRxiv. **2** (2020) 2. https://doi.org/10.1101/2020.02.26.20028373

24 K. K Patel and S. M Patel: IJESC. **6** (2016) 1. https://doi.org/10.4010/2016.1482
25 GraphPad Software: https://www.graphpad.com/guides/prism/latest/statistics/sensitivity_and_specificity.htm (accessed Feb 2023).
26 V. L. D. Thi, K. Herbst, K. Boerner, M. Meurer, L. P. M. Kremer, D. Kirrmaier, A. Freistaedter, D. Papagiannidis, C. Galmossi, M. L. Stanifer, S. Boulant, S. Klein, P. Chlanda, D. Khalid, I. B. Miranda, P. Schnitzler, H. G. Krausslich, M. Knop, and S. Anders: Sci. Transl. Med. **12** (2020) 4. https://doi.org/10.1126/scitranslmed.abc7075
27 M. N. Aoki, B. D. O. Coelho, L. G. B. Góes, P. Minoprio, E. L. Durigon, L. G. Morello, F. K. Marchini, I. N. Riediger, M. D. C. Debur, H. I. Nakaya, and L. Blanes: Sci. Rep. **11** (2021) 1. https://doi.org/10.1038/s41598-021-88506-y
28 L. Yu, S. Wu, X. Hao, X. Dong, L. Mao, V. Pelechano, W. H. Chen, and X. Yin: Clin. Chem. **66** (2020) 975. https://doi.org/10.1093/clinchem/hvaa102
29 V. M. Corman, O. Landt, M. Kaiser, R. Molenkamp, A. Meijer, D. K. W. Chu, T. Bleicker, S. Brunink, J. Schneider, M. L. Schmidt, D. G. J. C. Mulders, B. L. Haagmans, B. V. D. Veer, S. V. D. Brink, L. Wijsman, G. Goderski, J. L. Romette, J. Ellis, M. Zambon, M. Peiris, H. Goosens, C. Reusken, M. P. G. Koopmans, and C. Drosten: Euro Surveill. **25** (2020) 1. https://doi.org/10.2807%2F1560-7917.ES.2020.25.3.2000045
30 H. Benrahma, I. Diawara, I. Smyej, J. Rahoui, N. Meskaouni, R. Benmessaoud, A. Khadija, J. Khadija, M. F. Zahra, A. Zahra, N. Salma, E. Hajar, J. Leila, O. Fadoua, E. L. B. Jalila, and N. Chakib: medRxiv. **2** (2020) 10. https://www.medrxiv.org/content/10.1101/2020.06.18.20135137v1
31 Y. Dong, Y. Zhao, S. Li, Z. Wan, R. Lu, X. Yang, G. Yu, J. Reboud, J. M. Cooper, Z. Tian, and C. Zhang: ACS Sens. **7** (2022) 730. https://doi.org/10.1021/acssensors.1c02079
32 W. S. Jang, D. H. Lim, J. Yoon, A. Kim, M. Lim, J. Nam, R. Yanagihara, S. W. Ryu, B. K. Jung, N. H. Ryoo, and C. S. Lim: PloS One. **16** (2021) 1. http://dx.doi.org/10.1371/journal.pone.0248042
33 N. D. Zakaria, M. H. Omar, N. N. Ahmad Kamal, K. Abdul Razak, T. Sönmez, V. Balakrishnan, and H. H. Hamzah: ACS Omega. **6** (2021) 24419. https://doi.org/10.1021/acsomega.1c02670
34 M. Drobysh, V. Liustrovaite, A. Baradoke, R. Viter, C. F. Chen, A. Ramanavicius, and A. Ramanaviciene: Biosens. **12** (2022) 3. https://doi.org/10.3390/bios12080593
35 H. Y. Kim, J. H. Lee, M. J. Kim, S. C. Park, M. Choi, W. Lee, K. B Ku, B. T. kim, E. C. Park, H. G. Kim, and S. I. Kim: Biosens. **175** (2021) 1. https://doi.org/10.1016/j.bios.2020.112868
36 M. Johnston, H. C. Ates, R. T. Glatz, H. Mohsenin, R.Schmachtenberg, N. Göppert, D. Huzly, G. A. Urban, W. Waber, and C. Dincer: Mater. Today. **61** (2022) 129. https://doi.org/10.1016/j.mattod.2022.11.001

Supplementary Table 1

No.	Sample labels	ID sample	C_t value			RT-LAMP assay	$^{6}I_p$ (μA)	$^{7}\Delta I$ (μA)
			IC	RdRp gene	E gene			
1	[1]PS1	215196	27.89	20.51	20.56	[4]1	2.63	1.62
2	PS2	215197	30.1	38.23	36.63	1	2.97	1.28
3	PS3	215199	28.21	25.51	25.84	1	3.26	0.99
4	PS4	215200	27.63	36.86	32.1	[5]0	3.31	0.94
5	PS5	215201	28.74	24.41	24.44	1	2.61	1.64
6	PS6	215203	28.99	31.36	31.41	1	2.75	1.5
7	PS7	215204	29.24	27.51	28.07	1	2.44	1.81
8	[2]NS1	216139	30.16	[3]N/A	N/A	0	3.27	0.98
9	NS2	216150	28.08	N/A	N/A	0	3.7	0.55
10	NS3	216140	31.25	N/A	N/A	1	3.89	0.36
11	NS4	216136	33.21	N/A	N/A	0	3.93	0.32
12	NS5	216141	28.27	N/A	N/A	0	3.57	0.68
13	NS6	216113	31.1	N/A	N/A	0	3.39	0.86
14	NS7	216118	31.94	N/A	N/A	0	3.35	0.9
15	PS8	215169	24.23	22.35	22.27	1	3.15	1.37
16	PS9	215193	28.42	31.61	31.58	0	3.09	1.43
17	PS10	215195	30.51	27.87	27.6	0	3.09	1.43
18	PS11	215206	25.59	24.15	23.95	1	3.5	1.02
19	PS12	215216	23.31	21.11	20.65	1	3.08	1.44

Supplementary Table 1 (Continued)

No.	Sample labels	ID sample	C_t value			RT-LAMP assay	$^{6}I_p$ (μA)	$^{7}\Delta I$ (μA)
			IC	RdRp gene	E gene			
20	NS8	213579	26.02	N/A	N/A	0	3.35	1.17
21	NS9	213547	27.66	N/A	N/A	0	3.9	0.62
22	NS10	216149	30.2	N/A	N/A	0	3.92	0.6
23	NS11	216119	31.06	N/A	N/A	0	3.61	0.91
24	NS12	216414	26.09	N/A	N/A	0	3.49	1.03
25	PS13	214354	27.47	23.33	23.33	1	3.09	1.4
26	PS14	214361	28.75	30.72	30.71	0	2.96	1.53
27	PS15	214394	29.3	20.8	20.89	1	3.2	1.29
28	PS16	214395	27.97	27.07	27.11	0	2.82	1.67
29	PS17	214397	28.68	25.38	25.49	1	2.87	1.62
30	NS13	213581	30.74	N/A	N/A	0	3.32	1.17
31	NS14	213564	31.25	N/A	N/A	0	3.89	0.6
32	NS15	213578	28.26	N/A	N/A	0	3.11	1.38
33	NS16	213562	28.66	N/A	N/A	0	3.49	1
34	NS17	213568	29.46	N/A	N/A	0	3.36	1.13
35	PS18	213582	25.35	21.67	21.17	1	3.36	0.67
36	PS19	214328	28.21	24.13	23.85	0	2.51	1.52
37	PS20	214337	28.7	24.55	24.21	1	3.51	0.52
38	PS21	214340	27.18	24.03	23.59	0	3.34	0.69
39	PS22	214400	28.28	24.97	24.61	1	2.75	1.28
40	PS23	214436	31.15	30.53	30.22	1	2.91	1.12
41	NS18	213571	29.22	N/A	N/A	0	3.55	0.48
42	NS19	213575	29.2	N/A	N/A	0	3.79	0.24
43	NS20	213554	29.51	N/A	N/A	0	3.84	0.19
44	NS21	213531	29.48	N/A	N/A	0	3.86	0.17
45	NS22	213536	30.16	N/A	N/A	0	3.8	0.23
46	NS23	213563	26.71	N/A	N/A	0	3.5	0.53
47	PS24	215297	28.47	23.58	23.29	1	3.51	1.16
48	PS25	215301	29.04	31.99	31.55	0	3.32	1.35
49	PS26	215305	27.97	20.69	20.59	1	3.19	1.48
50	PS27	215308	24.78	19.76	19.49	1	3.85	0.82
51	PS28	215312	28.65	29.33	29.31	1	3.64	1.03
52	NS24	216068	28.72	N/A	N/A	0	3.63	1.04
53	NS25	216067	30.22	N/A	N/A	0	4.08	0.59
54	NS26	216100	33.63	N/A	N/A	0	3.79	0.88
55	NS27	216102	26.23	N/A	N/A	0	4.21	0.46
56	NS28	216063	30.71	N/A	N/A	0	3.73	0.94
57	PS29	215318	28.29	24.23	24.42	1	3.75	0.78
58	PS30	215328	30.04	27.15	27.52	1	3.82	0.71
59	PS31	215714	26.37	20.98	21.27	1	3.72	0.81
60	PS32	215717	28.44	23.85	24.15	1	3.65	0.88
61	PS33	215754	31.65	32.86	33.61	0	3.34	1.19
62	NS29	216098	28.53	N/A	N/A	0	3.83	0.7
63	NS30	216075	27.4	N/A	N/A	0	4.04	0.49
64	NS31	216074	29.16	N/A	N/A	0	4.32	0.21
65	NS32	216033	26.68	N/A	N/A	0	3.86	0.67
66	NS33	216071	28.53	N/A	N/A	0	4.07	0.46
67	PS34	215764	30.34	34.78	34.6	0	3.32	1.38
68	PS35	215766	27.47	35.74	34.11	0	3.54	1.16
69	PS36	215769	28.93	34.27	34.03	1	2.94	1.76

Supplementary Table 1 (Continued)

No.	Sample labels	ID sample	C_t value			RT-LAMP assay	$^{6}I_p$ (μA)	$^{7}\Delta I$ (μA)
			IC	RdRp gene	E gene			
70	PS37	215774	30.44	25.53	25	1	3.27	1.43
71	PS38	215784	28.52	27.06	26	1	3.25	1.45
72	NS34	216148	29.1	N/A	N/A	0	4.36	0.34
73	NS35	216105	32.11	N/A	N/A	0	4.52	0.18
74	NS36	214512	30.68	N/A	N/A	0	4.59	0.11
75	NS37	214891	30.98	N/A	N/A	0	4.56	0.14
76	NS38	214907	30.12	N/A	N/A	0	3.71	0.99
77	PS39	215795	32.07	33.48	33.31	1	2.9	1.82
78	PS40	215804	32.8	34.25	34.17	0	3.08	1.64
79	PS41	215807	32.59	31.25	31.18	1	3.67	1.05
80	PS42	215812	28.95	32.07	31.89	0	3.44	1.28
81	NS39	215729	28.14	N/A	N/A	0	4.61	0.11
82	NS40	215768	27.16	N/A	N/A	0	3.93	0.79
83	NS41	215788	29.13	N/A	N/A	0	3.94	0.78
84	NS42	215789	30.56	N/A	N/A	0	4.51	0.21
85	PS43	215814	31.15	24.87	24.73	1	3.64	1.15
86	PS44	215816	29.57	34.31	33.9	0	3.34	1.45
87	PS45	215823	29.99	21.77	21.75	1	3.96	0.83
88	PS46	216062	29.78	30.14	29.95	1	3.34	1.45
89	PS47	216064	28.79	20.21	20.12	1	4.11	0.68
90	PS48	216066	24.6	21.49	21.5	1	3.96	0.83
91	PS49	216070	30.39	36.13	36.82	0	3.73	1.06
92	NS43	213519	30.71	N/A	N/A	0	3.92	0.87
93	NS44	213520	29.74	N/A	N/A	0	3.96	0.83
94	NS45	215551	32.74	N/A	N/A	0	4.64	0.15
95	NS46	215718	32.17	N/A	N/A	0	4.16	0.63
96	NS47	215728	27.94	N/A	N/A	0	3.97	0.82
97	NS48	215738	29.05	N/A	N/A	0	4.23	0.56
98	NS49	215787	30.21	N/A	N/A	0	4.24	0.55
99	PS50	216072	24.1	19.18	18.67	1	3.5	1.09
100	PS51	216073	29.91	36.38	35.12	0	3.31	1.28
101	PS52	216078	28.6	20.82	20.51	1	3.63	0.96
102	PS53	216081	32.1	20.1	19.89	1	3.15	1.44
103	PS54	216084	27.92	34.73	35.03	0	3.01	1.58
104	PS55	216085	30.81	26.17	25.93	1	3.53	1.06
105	NS50	215802	30.52	N/A	N/A	0	3.87	0.72
106	NS51	215798	33.47	N/A	N/A	0	4.38	0.21
107	NS52	213538	30.07	N/A	N/A	0	4.2	0.39
108	NS53	213510	30.83	N/A	N/A	0	3.38	1.21
109	NS54	213508	30.72	N/A	N/A	0	3.92	0.67
110	NS55	215759	29.36	N/A	N/A	0	3.89	0.7
111	PS56	216079	26.08	29.18	29.6	1	2.6	1.54
112	PS57	216086	28.53	27.05	27.83	1	2.88	1.26
113	PS58	216087	30.13	33.54	28.94	0	2.09	2.05
114	PS59	216088	28.94	31.01	31.22	1	2.42	1.72
115	PS60	216089	29.31	25.56	26.18	1	3.17	0.97
116	PS61	216090	28.34	32.19	32.9	0	2.7	1.44
117	NS56	215797	31.41	N/A	N/A	0	3.42	0.72
118	NS57	213527	29.51	N/A	N/A	0	3.3	0.84
119	NS58	213518	23.81	N/A	N/A	0	3.48	0.66

Supplementary Table 1 (Continued)

No.	Sample labels	ID sample	C_t value			RT-LAMP assay	[6]I_p (μA)	[7]ΔI (μA)
			IC	RdRp gene	E gene			
120	NS59	213500	29.85	N/A	N/A	0	3.23	0.91
121	NS60	215726	29.78	N/A	N/A	0	3.23	0.91
122	NS61	215736	27.58	N/A	N/A	0	3.66	0.48
123	PS62	216092	31.95	30.35	30.42	0	3.07	1.14
124	PS63	216097	30.25	34.43	35.65	0	2.9	1.31
125	PS64	216099	25.78	21.1	21.63	1	2.81	1.4
126	PS65	216103	29.87	18.6	19.26	1	2.39	1.82
127	NS62	215735	29.76	N/A	N/A	0	3.29	0.92
128	NS63	215745	26.44	N/A	N/A	0	3.27	0.94
129	NS64	215800	27.02	N/A	N/A	0	3.35	0.86
130	NS65	215776	24.8	N/A	N/A	0	2.94	1.27
131	PS66	216095	30.46	25.72	25.75	1	3.91	0.72
132	PS67	216101	25.04	21.89	21.92	1	3.08	1.55
133	PS68	216122	30.03	22.54	22.78	1	3.31	1.32
134	PS69	216129	27.37	27.27	27.35	1	2.17	2.46
135	NS66	213514	30.08	N/A	N/A	0	4.06	0.57
136	NS67	213516	27.92	N/A	N/A	0	3.96	0.67
137	NS68	213513	30.04	N/A	N/A	0	4.1	0.53
138	NS69	215799	28.49	N/A	N/A	0	3.94	0.69
139	PS70	216130	28.9	28.82	27.7	1	2.98	1.4
140	PS71	213132	31.06	19.07	17.98	1	3.12	1.26
141	PS72	213135	27.22	18.32	17.25	1	3.55	0.83
142	PS73	213561	25.84	27.75	26.51	1	2.83	1.55
143	PS74	213556	30.94	32.95	32.36	0	2.56	1.82
144	NS70	215744	29.18	N/A	N/A	0	3.86	0.52
145	NS71	215765	30.05	N/A	N/A	0	4.1	0.28
146	NS72	215785	30.19	N/A	N/A	0	4.32	0.06
147	NS73	215724	28.95	N/A	N/A	0	4.24	0.14
148	NS74	215734	30.71	N/A	N/A	0	4.34	0.04

[*1]PS, positive sample
[*2]NS, negative sample
[*3]N/A, not available
[*4]1, color changes from pink to yellow
[*5]0, color remains pink
[*6]I_p (μA), peak height
[*7]ΔI (μA), delta I